Efficient control of connected and automated vehicles on a two-lane highway with a moving bottleneck

Huaqing Liu(刘华清) and Rui Jiang(姜锐)†

Key Laboratory of Transport Industry of Big Data Application Technologies for Comprehensive Transport, Ministry of Transport, Beijing Jiaotong University, Beijing 100044, *China*

(Received 12 December 2022; revised manuscript received 19 January 2023; accepted manuscript online 6 February 2023)

This paper investigates the traffic flow of connected and automated vehicles (CAVs) inducing by a moving bottleneck on a two-lane highway. A heuristic rules-based algorithm (HRA) has been used to control the traffic flow upstream of the moving bottleneck. In the HRA, some CAVs in the control zone are mapped onto the neighboring lane as virtual ones. To improve the driving comfort, the command acceleration caused by virtual vehicle is restricted. Comparing with the benchmark in which the CAVs change lane as soon as the lane changing condition is met, the HRA significantly improves the traffic flow: the overtaking throughput as well as the outflow rate increases, the travel delay and the fuel consumption decrease, the comfort level could also be improved.

Keywords: traffic flow, connected and automated vehicles, moving bottleneck

PACS: 45.70.Vn, 89.40.Bb, 05.70.Fh, 64.60.Cn **DOI:** 10.1088/1674-1056/acb918

1. Introduction

The deployment of connected and automated vehicles (CAVs) is regarded as an effective method to increase traffic capacity[1] and reduce energy consumption.[2] In particular, at the bottlenecks, CAVs are able to maximize the utilization of spaces[3] and smooth traffic oscillations.

Bottlenecks can be classified into fixed ones and moving ones. The fixed ones include the merges, diverges, weaving areas, and so on. The merging algorithms of CAVs at the merges are widely investigated.[4–8] One typical control method to adjust the merging state is heuristic rules-based algorithm (HRA).[9–11] Some heuristic rules are introduced to assist in adjusting the longitudinal driving and lane-changing of CAVs. For example, in Ref. [12], by mapping a vehicle on one lane onto another lane, a virtual vehicle was generated to make smooth merging. Simulation results exhibited the feasibility of this merging control algorithm. As an extension of this virtual vehicle algorithm, Lu and Hedrick[13] and Lu *et al.*[14] proposed the concept of virtual platoon, which can effectively avoid a two-point boundary value problem. Based on the concept, some field test with automated cars was carried out, which demonstrated it is a rather general adaptive algorithm. The other approach for the longitudinal control of CAVs at merges is optimization-based control algorithm.[15] Several optimization-based control algorithms have been formulated and the trajectories of CAVs with different objectives can be solved.[16] For example, the method utilizing the Hamilton function is used in Ref. [17] to obtain the analytic solution of the trajectory with the objective to minimize the combined cost function consisting of the acceleration, the jerk and the time-derivative of jerk. Another widely used optimization-based control is proposed in Ref. [18], which maximizes average travel velocity of the vehicles.

The diverging of CAVs has also been studied.[19,20] Learning-based algorithm is one typical control method to control the lane changing behavior at diverges.[21,22] Considering the farsighted lane-changing behavior, a new cooperative lane-changing strategy was developed in Ref. [23] based on the reinforcement learning technique. The simulation showed that the traffic flow and traffic speed have been improved. The HRA has also been used to coordinate the through vehicles and the exiting vehicles in an efficient manner.[24,25] For example, based on the relaxation effect, Zheng *et al.*[26] modified the minimizing overall braking induced by lane changes model (MOBIL) to control the diverging vehicles and cooperative vehicles to tolerate shorter gaps when a lane change is executed. The simulation result showed that the proposed HRA could improve traffic operation, traffic safety, and traffic oscillation.

The weaving area usually consists of a merge at upstream and a diverge at downstream.[27] Interactions of vehicles at weaving area are more complex than that at merges and diverges. The HRA is also a typical and effective control method to coordinate the merging vehicles, the diverging vehicles and the through vehicles. For example, Subraveti *et al.*[28] proposed a control strategy to organize traffic flow well upstream of a bottleneck by assigning CAVs across lanes, which can reduce the flow rate near the bottleneck to increase the overtaking throughput. Also some optimization based algorithms were proposed to solve the trajectories of vehicles inside the

†Corresponding author. E-mail: jiangrui@bjtu.edu.cn

© 2023 Chinese Physical Society and IOP Publishing Ltd

control zone. For example, Yang *et al.*[29] proposed a dynamic programming approach and utilized a relaxation-based approximate algorithm to obtain a suggested lane-changing gap and a reference longitudinal trajectory. The simulation showed that there is a substantial improvement on traffic efficiency and passengers' experiences. Finally, learning-based algorithms can also be utilized in the weaving area. For example, Zhu[30] used the deep reinforcement learning to investigate several driving strategies at weaving area in SUMO traffic simulations. The results indicated that the proposed algorithm can mitigate traffic congestion and propagation of shockwaves but lead to a poorer passenger comfort.

On the other hand, moving bottlenecks are usually caused by slow vehicles.[31,32] The impact of moving bottlenecks is widely investigated in conventional traffic flow. For example, Fang *et al.*[33] investigated the effect of moving bottleneck on a two-lane traffic flow and the results demonstrated that the effect of moving bottleneck enlarges with the increase of inflow rate, but it can be reduced by increasing the maximum velocity of slow vehicle. Hu *et al.*[34] investigated the influence of moving bottleneck on tidal lane at a bidirectional six-lane motorway. The simulation showed that the low-speed moving bottleneck will cause the speed interference to merging. With the aim to reduce the negative traffic impacts of slow vehicles in urban environments, Simoni *et al.*[35] proposed a new semi-analytic numerical scheme to determine the trajectories of all moving bottlenecks accurately and fast. The results of application in two different optimization problems exhibit that this algorithm reduces the computing time by 8%–17%.

Comparing with the vast studies on traffic flow of CAVs induced by fixed bottlenecks, the study concerning traffic flow induced by moving bottleneck is lacked. To our knowledge, the only related study is reported in Ref. [36], in which a CAV is treated as a moving bottleneck and its velocity is assumed as control variable of a model prediction control algorithm that aims to minimize travel times. The simulation results showed that it is able to significantly reduce the occurrence of capacity drop.

Motivated by the fact, this paper aims to study how to improve traffic flow of CAVs induced by moving bottlenecks. To this end, an HRA has been used in the control zone, which moves with the moving bottleneck. It is shown that comparing with the benchmark scenario in which the CAVs change lane as soon as the lane changing condition is met, the HRA remarkably could improve the overtaking throughput, the travel delay, the fuel consumption, and the comfort level.

The rest of the paper is organized as follows. In Section 2, the control algorithm as well as the lanechanging rules in the benchmark is introduced. Section 3 compares the performance of the HRA with that of the benchmark. Section 4 gives the conclusion.

2. The HRA and the benchmark

2.1. Geometric layout and assumptions

Figure 1 shows the geometric layout of a moving bottleneck on a two-lane highway. As in Refs. [37,38], we assume that inflow rate is the same on the two lanes. The moving bottleneck moves at a constant velocity and the control zone moves with the moving bottleneck at the same speed. All vehicles on lane 1 need to change into lane 2. After overtaking the moving bottleneck, the vehicles are redistributed evenly into the two lanes.

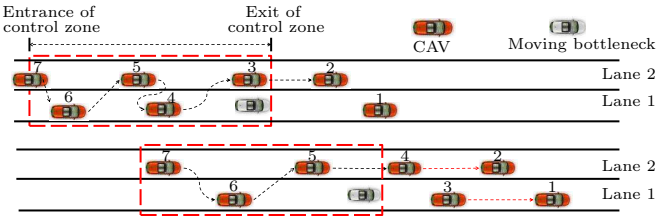


Fig. 1. The geometric layout of a moving bottleneck on a two-lane highway.

2.2. Longitudinal control algorithm outside control zone

As in Refs. [37–42], we assume that a CAV follows its preceding one outside control zone with a constant time gap control algorithm, in which the command acceleration and the actual acceleration are

$$a_{\mathrm{cmd}} = k_{\mathrm{a}} a_{\mathrm{p}} + k_{\mathrm{v}} \left(v_{\mathrm{p}} - v\right) + k_{\mathrm{g}} \left(g - g_{\mathrm{desire}}\right), \tag{1}$$

$$a + \tau \dot{a} = a_{\mathrm{cmd}}, \tag{2}$$

where a_{cmd} consists of three parts: (i) the acceleration of the preceding vehicle; (ii) the speed difference between the preceding vehicle and the ego vehicle; (iii) the spacing difference between the actual spacing and the desired spacing. g is the actual spacing and g_{desire} is the desired spacing

$$g = x_{\mathrm{p}} - x, \tag{3}$$

$$g_{\mathrm{desire}} = L + G_{\min} + T_{\mathrm{g}} v. \tag{4}$$

Moreover, the physical constraints below should be satisfied

$$v_{\min} \le v \le v_{\max}, \tag{5}$$

$$a_{\min} \le a_{\mathrm{cmd}} \le a_{\max}, \tag{6}$$

$$J_{\min} \le J \le J_{\max}, \tag{7}$$

$$g \ge v T_{\mathrm{safe}} + L + G_{\min} \tag{8}$$

in which $J = \mathrm{d}a/\mathrm{d}t$ is the jerk of vehicle. Other notations and parameters are listed in Table 1.

When the CAVs enter the control zone, their merging sequence is determined by 'first-in-first-out' (FIFO) principle. If two CAVs enter at the same time instant, the one on lane 1 is regarded as the 'first-in' one.

Table 1. Notations and parameters.

Notations	Description
$a_{\rm p}$	acceleration of preceding vehicle
$v_{\rm p}$	velocity of preceding vehicle
$x_{\rm p}$	location of preceding vehicle
a	acceleration of ego vehicle
v	velocity of ego vehicle
x	location of ego vehicle
Parameters	**Description**
$k_{\rm a}$, $k_{\rm v}$, $k_{\rm g}$	control gains
$T_{\rm g}$, τ, $T_{\rm safe}$	desired time gap, time delay, safe time gap
L, $G_{\rm min}$	length of vehicle and standstill gap

2.3. Control algorithms in control zone

We briefly review the HRA proposed in Ref. [37]. When a CAV enters the control zone, its traffic information is added in a virtual set, which includes all vehicles in the control zone. The sequence of these vehicles in the virtual set is numbered based on the arriving order at the control zone. If two vehicles arrive at the control zone at the same time, vehicle from lane 1 is numbered before that from lane 2. In the virtual set, if the preceding vehicle of the ego one is not on the same lane, then we map the preceding vehicle onto the ego lane, which becomes a virtual leading vehicle of the ego one. For an example of the virtual vehicle, see Fig. 2. Note that if the preceding vehicle of the ego one is on the same lane, then the ego vehicle has no virtual leading vehicle.

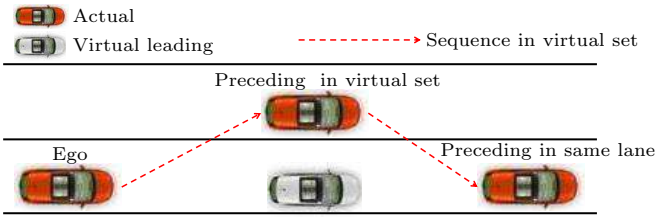


Fig. 2. An example sketch of the virtual vehicle.

The command acceleration $a_{\rm cmd,ego}$ of ego vehicle concerning vehicle on the same lane is calculated as

$$a_{\rm cmd,ego} = k_{\rm a}a_{\rm p,ego} + k_{\rm v}\left(v_{\rm p,ego} - v\right) + k_{\rm g}\left(g_{\rm ego} - g_{\rm desire}\right). \quad (9)$$

The command acceleration $a_{\rm cmd,virtual}$ concerning virtual leading vehicle is calculated as

$$\begin{aligned} a_{\rm cmd,virtual} = \max\big(&k_{\rm a}a_{\rm p,virtual} + k_{\rm v}\left(v_{\rm p,virtual} - v\right) \\ &+ k_{\rm g}\left(g_{\rm virtual} - g_{\rm desire}\right), a_{\rm cmd,lim}\big), \end{aligned} \quad (10)$$

where $a_{\rm cmd,lim}$ is the restriction on $a_{\rm cmd,virtual}$ to improve driving comfort level.

The command acceleration for vehicles that have a virtual leading vehicle, is determined as

$$a_{\rm cmd} = \min(a_{\rm cmd,ego}, a_{\rm cmd,virtual}). \quad (11)$$

For vehicles that have no virtual leading vehicle, $a_{\rm cmd} = a_{\rm cmd,ego}$.

Inside the control zone, the physical constraints (5)–(8) should also be satisfied. Note that the longitudinal-lateral coupling [Eqs. (9)–(11)] is applied symmetrically for the vehicles on both lanes.

To make full use of the spacing, the lane-changing is implemented when the distance to the moving bottleneck is equal to $v_{\rm max}T_{\rm g} + L + G_{\rm min}$. Note that if the control zone is long enough, the vehicles will be able to adequately adjust their speed and location before reaching the lane changing location. Thus, when the vehicles on lane 2 change to lane 1, they can change lane safely and smoothly. The movement of vehicles on lane 1 will not be affected. When the vehicles overtake the moving bottleneck and are about to change to lane 1, the time gap to the moving bottleneck should also be larger than or equal to $T_{\rm safe}$.

2.4. The benchmark

In the benchmark, once the CAVs enter the control zone, the lane changing will be implemented as long as both time gaps to the preceding vehicle and the following vehicle on the target lane are larger than or equal to $T_{\rm safe}$, see Fig. 3. Moreover, lane changing can also be implemented outside the control zone if the velocity of a CAV is smaller than $v_{\rm max}$. This additional rule is used to balance the flow in the two lanes when traffic flow becomes congested.

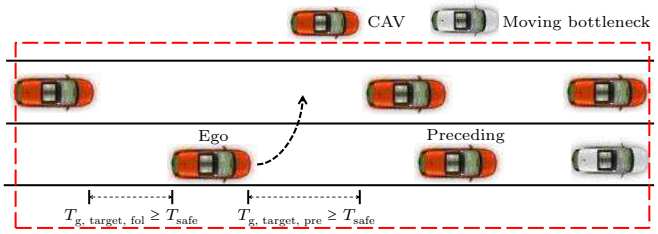


Fig. 3. The lane-changing in the benchmark scenario.

3. Evaluation of the control algorithm

The lengths of the studied road section and control zone are set to 20 km and 2 km, respectively. The control zone is long enough to ensure the smooth and safe lane change of CAVs on lane 2. The inflows are stochastic. A vehicle enters with $v_{\rm max} = 30$ m/s and the probability p_0 if the last vehicle on the same lane is beyond $L + G_{\rm min} + T_{\rm g}v_{\rm max}$. By generating vehicles in this way, the headways of vehicles follow shifted negative exponential distribution, as observed in real traffic. When the leading vehicle reaches the exit at $x = 20$ km, it is removed and the second vehicle becomes the new leading one and its acceleration is assumed to be unchanged. In the simulation, 50 runs were carried out for each velocity of moving bottleneck. The results are averaged over the 50 runs. The

parameters used in the simulation are shown in Table 2. The control gain parameters should guarantee that traffic flow is stable, and other parameters are in the usual ranges reported in the literature, see Refs. [37,38,43–47].

Table 2. The values of parameters.

Parameters	Value	Parameters	Value
$J_{\min}$	-2 m/s^3	k_a	0.3
$J_{\max}$	2 m/s^3	k_v	1.5 s^{-1}
$a_{\min}$	-3 m/s^2	k_g	0.1 s^{-2}
$a_{\max}$	3 m/s^2	T_g	1.20 s
$v_{\min}$	0 m/s	T_{safe}	1.10 s
$v_{\max}$	30 m/s	τ	0.4 s
$G_{\min}$	2 m	L	5 m

3.1. Overtaking throughput and outflow rate

The number of vehicles overtaking the moving bottleneck per hour is defined as the overtaking throughput (q_{over}). Figure 4 shows the dependence of the overtaking throughput on entering probability p_0 at two typical velocities of moving bottleneck, which are $v_c = 10$ m/s and $v_c = 20$ m/s. One can see that overtaking throughput is independent of $a_{\text{cmd,lim}}$. Moreover, there exists a threshold of entering probability. When p_0 is smaller than the threshold, the traffic flow is free. When p_0 is larger than the threshold, the overtaking throughput becomes saturated, which implies that traffic congestion is induced by the moving bottleneck.

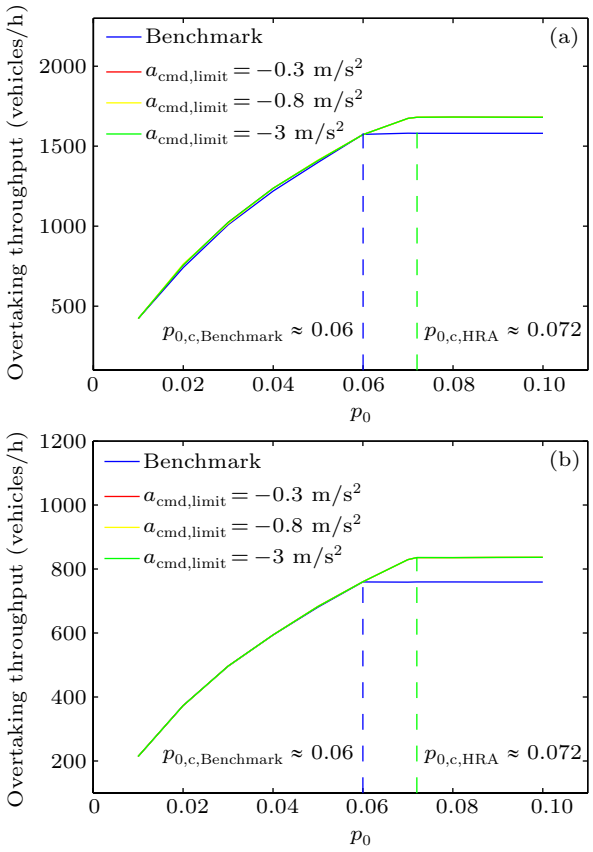


Fig. 4. The dependence of the overtaking throughput on the entering probability p_0 at $v_c = 10$ m/s (a), 20 m/s (b).

The two thresholds of overtaking throughput are $p_0 = p_{0,\text{c,HRA}} \approx 0.072$ under HRA and $p_0 = p_{0,\text{c,Benchmark}} \approx 0.06$ under benchmark. The saturated overtaking throughput equals to 1681 vehicles/h under HRA and 1581 vehicles/h under benchmark at $v_c = 10$ m/s, 837 vehicles/h under HRA, and 760 vehicles/h under benchmark at $v_c = 20$ m/s, respectively. Thus, under different v_c, HRA performs better than the benchmark in terms of capacity.

Figure 5 shows the saturated overtaking throughput at several other values of v_c. One can see that the saturated overtaking throughput under different $a_{\text{cmd,lim}}$ is also almost the same. Moreover, it decreases as v_c increases. Comparing with benchmark, the saturated overtaking throughput under the HRA is larger.

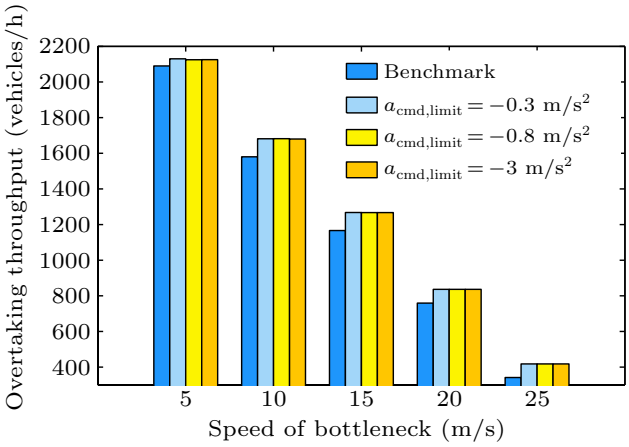


Fig. 5. The dependence of the saturated overtaking throughput on the speed of moving bottleneck.

Note that the threshold is independent of the speed of moving bottleneck. This can be understood as follows. We measure the outflow rate at the exit of the road. Figure 6 shows that the outflow is independent of v_c. Accordingly, the threshold of overtaking throughput is independent of v_c. Note that the maximum outflow rate is about 2522 vehicles/h under HRA, which is larger than 2365 vehicles/h under benchmark.

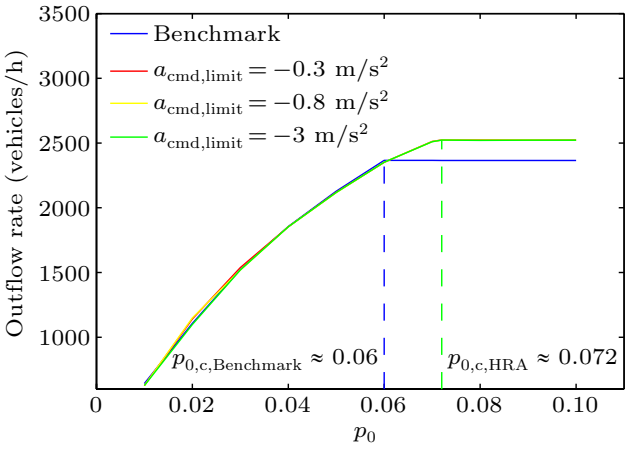


Fig. 6. The dependence of the outflow rate on the entering probability p_0. The result is independent of the speed of the moving bottleneck.

3.2. Spatiotemporal pattern

To understand evolution of the traffic flow induced by the moving bottleneck under the HRA and the benchmark, we study the spatiotemporal pattern of traffic flow. As an example, figure 7 shows the spatiotemporal patterns under the unsaturated inflow rate at $p_0 = 0.05$. To exhibit the traffic evolution in the control zone more clearly, we use a coordinate transformation and set $x_n(t) - v_c t$ as y coordinate, see Figs. 8–10. Here $x_n(t)$ denotes the location of vehicle n at time t.

Figure 8 shows the results in a typical low-level inflow rate at p_0 =0.05. Note that under the benchmark the spatiotemporal patterns in the two lanes are significantly different, see Figs. 8(c) and 8(f). In contrast, the patterns are similar in the two lanes under the HRA, see Figs. 8(a), 8(b), 8(d), and 8(e). One can see that there is a deceleration near control zone entrance when HRA is applied. However, the pattern is quite different under the benchmark. Just upstream of the moving bottleneck, traffic flow exhibits an alternate transition between free flow and congestion in lane 2 and it is in congestion in lane 1. The alternation in lane 2 is because CAVs on lane 1 sometimes are not able to change lane.

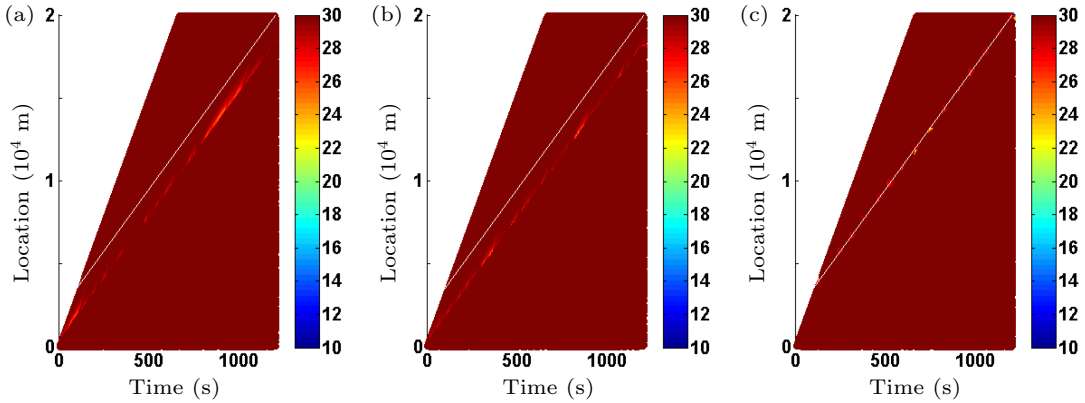


Fig. 7. The spatiotemporal pattern of speed (in units m/s) in lane 1 at $p_0 = 0.05$ with $v_c = 15$ m/s under (a) $a_{cmd,lim} = -0.3$ m/s^2, (b) $a_{cmd,lim} = -3$ m/s^2, (c) benchmark. The white line denotes the moving bottleneck.

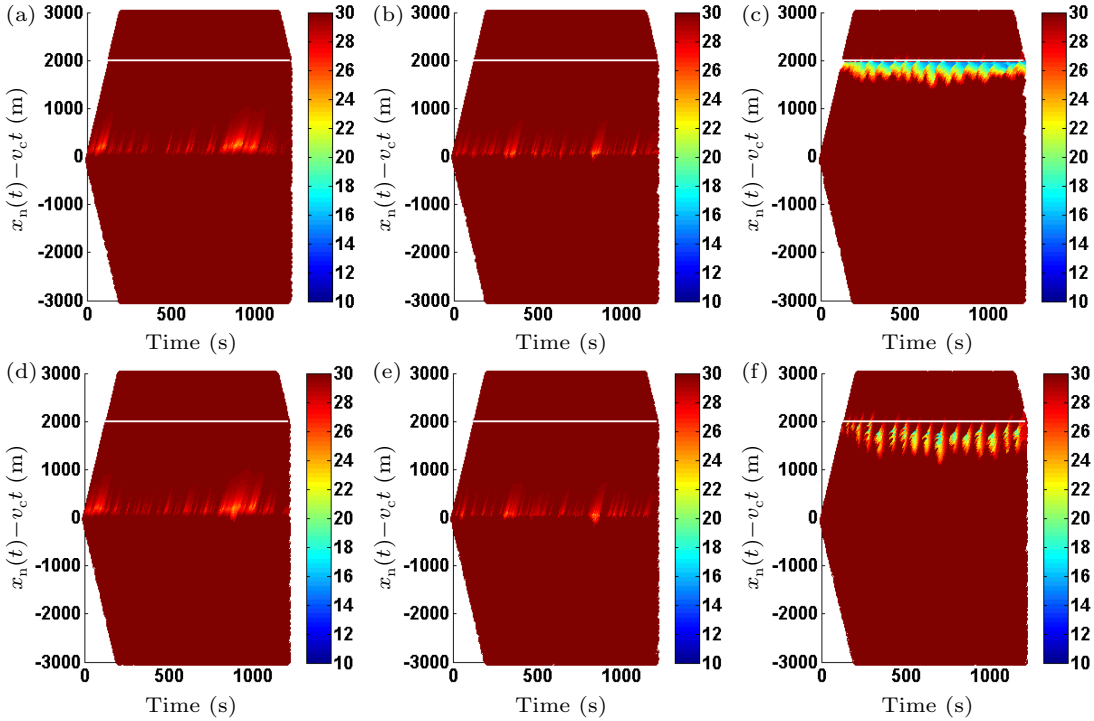


Fig. 8. The spatiotemporal pattern of speed (in units m/s) in panels (a)–(c) lane 1 and panles (d)–(f) lane 2 at $p_0 = 0.05$ with $v_c = 15$ m/s under panels (a) and (d) $a_{cmd,lim} = -0.3$ m/s^2, (b) and (e) $a_{cmd,lim} = -3$ m/s^2, (c) and (f) benchmark.

Figure 9 shows the result in a typical medium-level inflow rate at $p_0 = 0.065$. Under HRA, due to the stochastic inflow, although the mean inflow rate is smaller than the threshold of overtaking throughput, sometimes the local inflow rate on both lanes could exceed the threshold. Once the inflow exceeds the threshold, congestion occurs near control zone entrance. The congestion will dissipate when the local inflow rate falls below the threshold. Under the benchmark, the inflow exceeds the

threshold and congestion will occur and expand upstream. Nevertheless, the congestion initially emerges at the control zone exit rather than at the control zone entrance. Moreover, in lane 2, the congestion still alternates with the free flow.

Figure 10 shows the results in a typical high-level inflow rate at $p_0 = 0.09$. The inflow rate is beyond the thresholds and the congestions form in the traffic systems under both the HRA and the benchmark. Under the HRA, the congestion emerges at control zone entrance and then propagates upstream. Under the benchmark, the propagation of congestion is similar to that in the medium-level inflow rate situation.

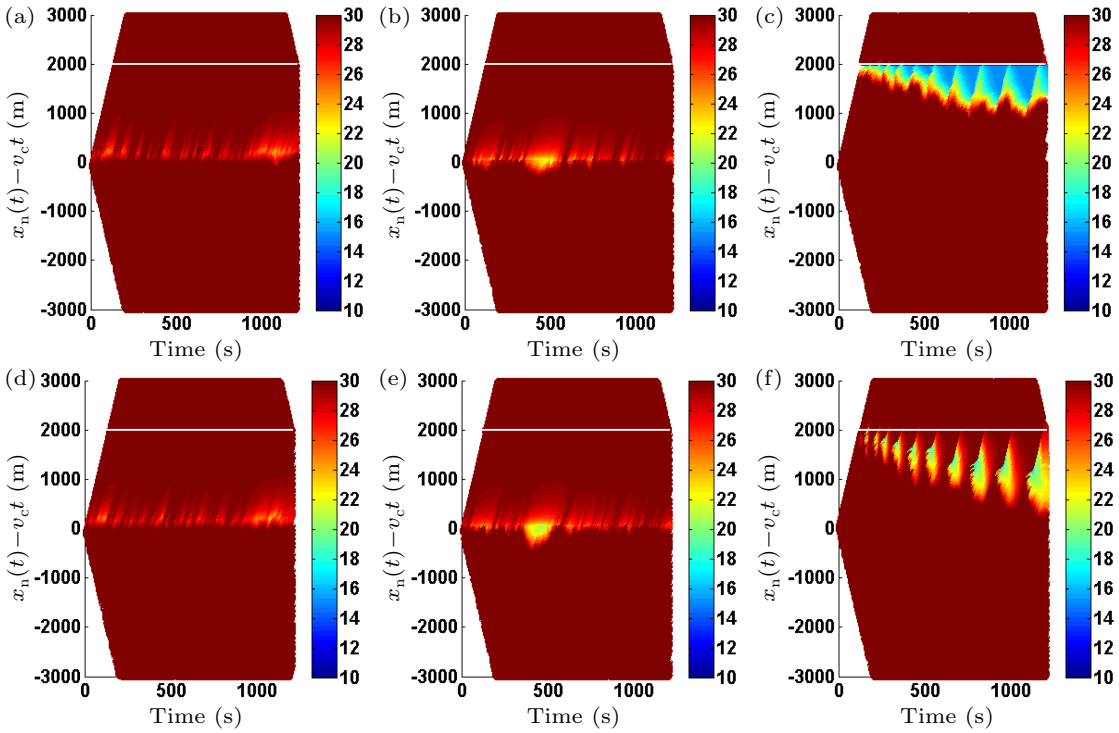


Fig. 9. The spatiotemporal pattern of speed (in units m/s) in panels (a)–(c) lane 1 and panels (d)–(f) lane 2 at $p_0 = 0.065$ with $v_c = 15$ m/s under panels (a) and (d) $a_{\text{cmd,lim}} = -0.3$ m/s^2, (b) and (e) $a_{\text{cmd,lim}} = -3$ m/s^2, (c) and (f) benchmark.

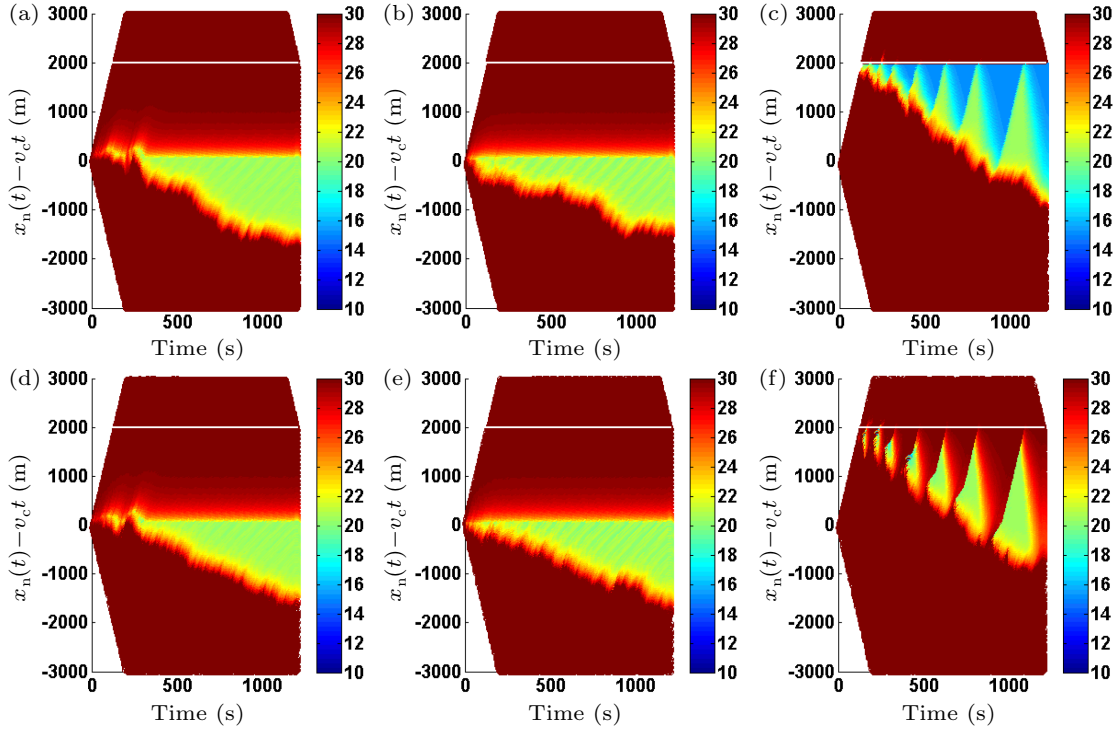


Fig. 10. The spatiotemporal pattern of speed (in units m/s) in panels (a)–(c) lane 1 and panels (d)–(f) lane 2 at $p_0 = 0.09$ with $v_c = 15$ m/s under (a) and (d) $a_{\text{cmd,lim}} = -0.3$ m/s^2, (b) and (e) $a_{\text{cmd,lim}} = -3$ m/s^2, (c) and (f) benchmark.

3.3. Travel delay

To measure the travel delay of ego vehicle, we define

$$\text{Delay} = t_{\text{e}} - t_0 - \frac{L_{\text{road}}}{v_{\max}}, \tag{12}$$

in which t_0 and t_{e} are the entering and leaving time of ego vehicle, respectively, L_{road} is the road length.

Figure 11 compares the dependence of the travel delay on p_0 and v_{c} between the HRA and the benchmark. One can see that no matter what v_{c} is, the travel delay under the benchmark is remarkably larger than that under the HRA, except at very small level of inflow. Moreover, the travel delay under the HRA is almost independent of $a_{\text{cmd,lim}}$. With the increase of v_{c}, the difference of travel delay between the HRA and the benchmark decreases.

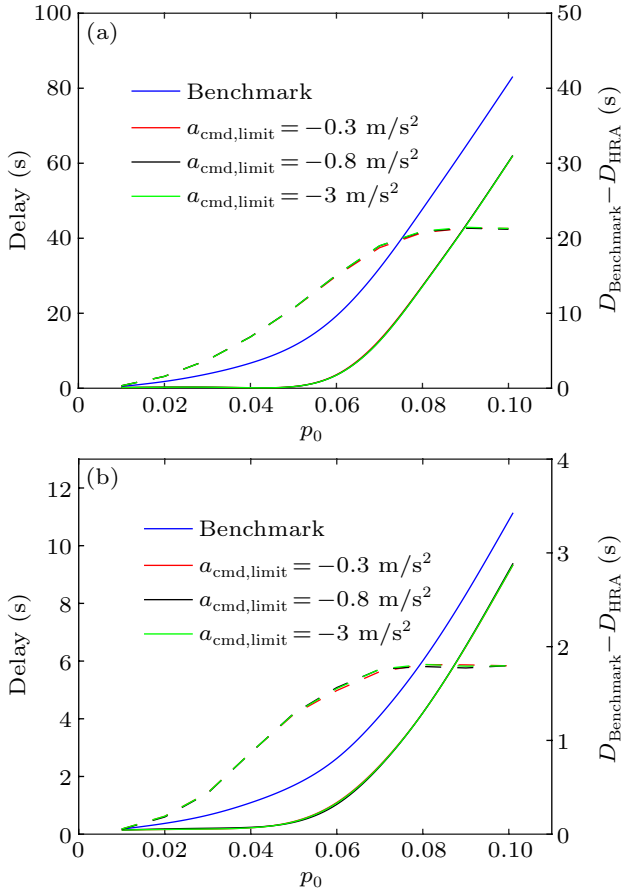


Fig. 11. The dependence of travel delay and its difference on the entering probability p_0 at $v_{\text{c}} = 10$ m/s (a), 20 m/s (b). Solid line: travel delay, dashed line: the difference of travel delay between benchmark and HRA.

3.4. Fuel consumption

To measure the fuel consumption (FC) of vehicles, we use the following model as in Refs. [48–50]

$$\text{FC}_i = \int_{t_0}^{t_{\text{e}}} \exp\left\{\sum_{i=0}^{3}\sum_{j=0}^{3} K_{ij}\,(a(t))^i\,(v(t))^j\right\} \text{d}t, \tag{13}$$

in which FC_i is the fuel consumption of vehicle i and K_{ij} is constant coefficients listed in Table 3.

Figure 12 compares the dependence of the fuel consumption on p_0 and v_{c} between the HRA and the benchmark. One can see that the fuel consumption increases with the inflow rate due to the formation of congestion. Under the HRA, larger $|a_{\text{cmd,lim}}|$ leads to higher fuel consumption. However, comparing with the benchmark, the fuel consumption under the HRA is always smaller. Moreover, the improvement is more remarkable at a smaller v_{c}.

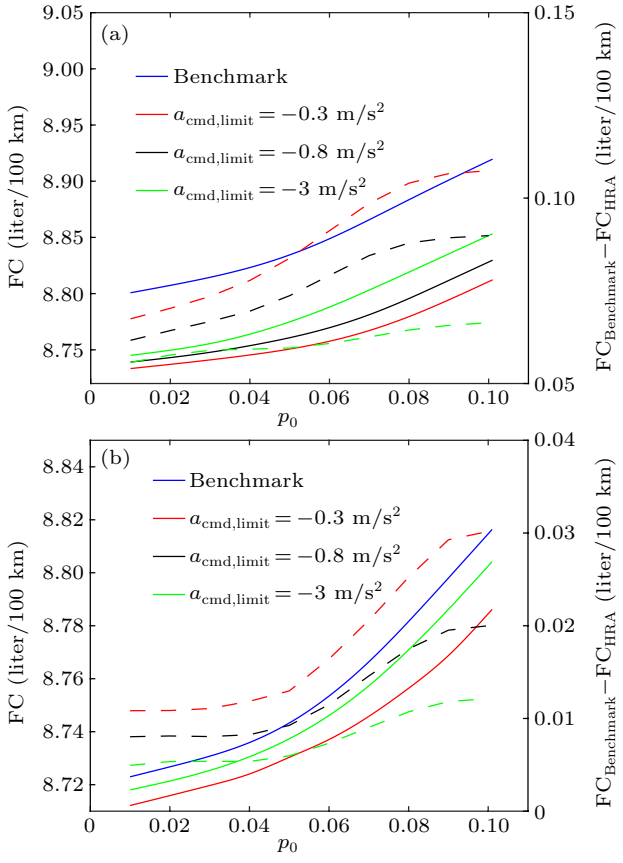


Fig. 12. The dependence of fuel consumption and its difference on the entering probability p_0 at $v_{\text{c}} = 10$ m/s (a), 20 m/s (b). Solid line: FC, dashed line: the difference of FC between benchmark and HRA.

Table 3. Coefficients of fuel consumption for $a \geq 0$ and $a < 0$.

K_{ij}	Positive acceleration				Negative acceleration			
	$j=0$	$j=1$	$j=2$	$j=3$	$j=0$	$j=1$	$j=2$	$j=3$
$i=0$	-7.735	0.2295	-5.61×10^{-3}	9.77×10^{-5}	-7.735	-0.01799	-4.27×10^{-3}	1.88×10^{-4}
$i=1$	0.02799	0.0068	-7.72×10^{-4}	8.38×10^{-6}	0.02804	7.72×10^{-3}	8.38×10^{-4}	3.39×10^{-5}
$i=2$	-2.23×10^{-4}	-4.40×10^{-5}	7.90×10^{-7}	8.17×10^{-7}	-2.20×10^{-4}	-5.22×10^{-5}	-7.44×10^{-6}	2.77×10^{-7}
$i=3$	1.09×10^{-6}	4.80×10^{-8}	3.27×10^{-8}	-7.79×10^{-9}	1.08×10^{-6}	2.47×10^{-7}	4.87×10^{-8}	3.79×10^{-10}

3.5. Comfort level

In the literature, J^2 is used to measure the instantaneous comfort level and the cumulative J^2 of each vehicle denotes the comfort level when driving through overall road section, see *e.g.*, Refs. [37,38,51]. We denote the cumulative J^2 as $\hat{J}^2$, thus

$$\hat{J}^2 = \int_{t_0}^{t_e} J^2 \mathrm{d}t. \tag{14}$$

A larger $\hat{J}^2$ means a lower comfort level.

Figure 13 compares the dependence of comfort level on p_0 and v_c between the HRA and the benchmark. One can see that (i) the comfort level under the HRA is no longer always better than that under the benchmark. However, the comfort level under $|a_{\mathrm{cmd,lim}}| = 0.3$ m/s^2 is still always better than that under the benchmark. (ii) the comfort level index under the HRA is monotonically increasing with the inflow, but the comfort level under the benchmark is not when v_c is small.

To understand the nonmonotonicity under the benchmark shown in Fig. 13(a), figure 14 shows the notable jerks with $|J| > 0.1$ m/s^3 under the benchmark at $v_c = 10$ m/s. When $p_0 \approx 0.04$, although the inflow is unsaturated, the congestion forms and occupies a rather wide region. The vehicles on lane 1 usually need to decelerate significantly and then change to lane 2. The vehicles on both lane 1 and lane 2 will experience an 'acceleration- deceleration' process frequently, which leads to a lower comfort level. With the further increase of inflow, the alternation pattern forms. As a result, the comfort level improves because vehicles cannot change lane in certain time periods.

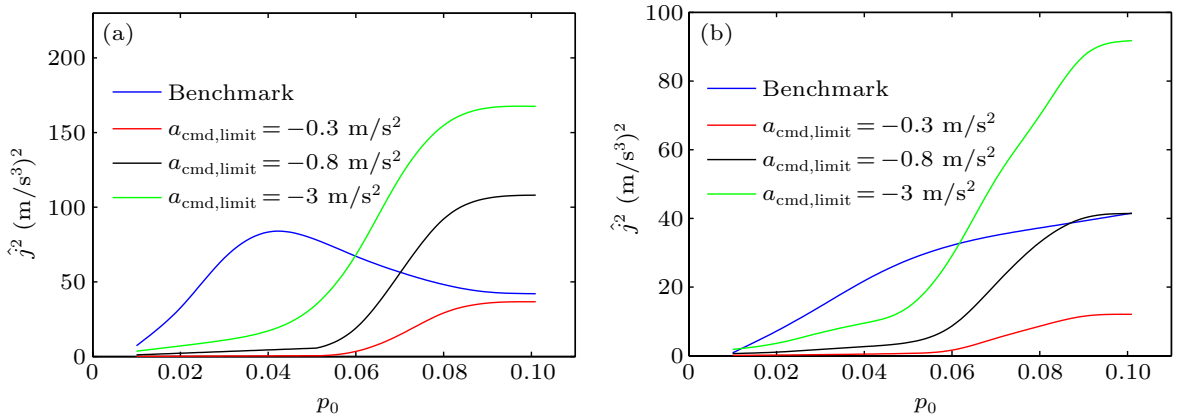


Fig. 13. The dependence of uncomfortable level on the entering probability p_0 at $v_c = 10$ m/s (a), 20 m/s (b).

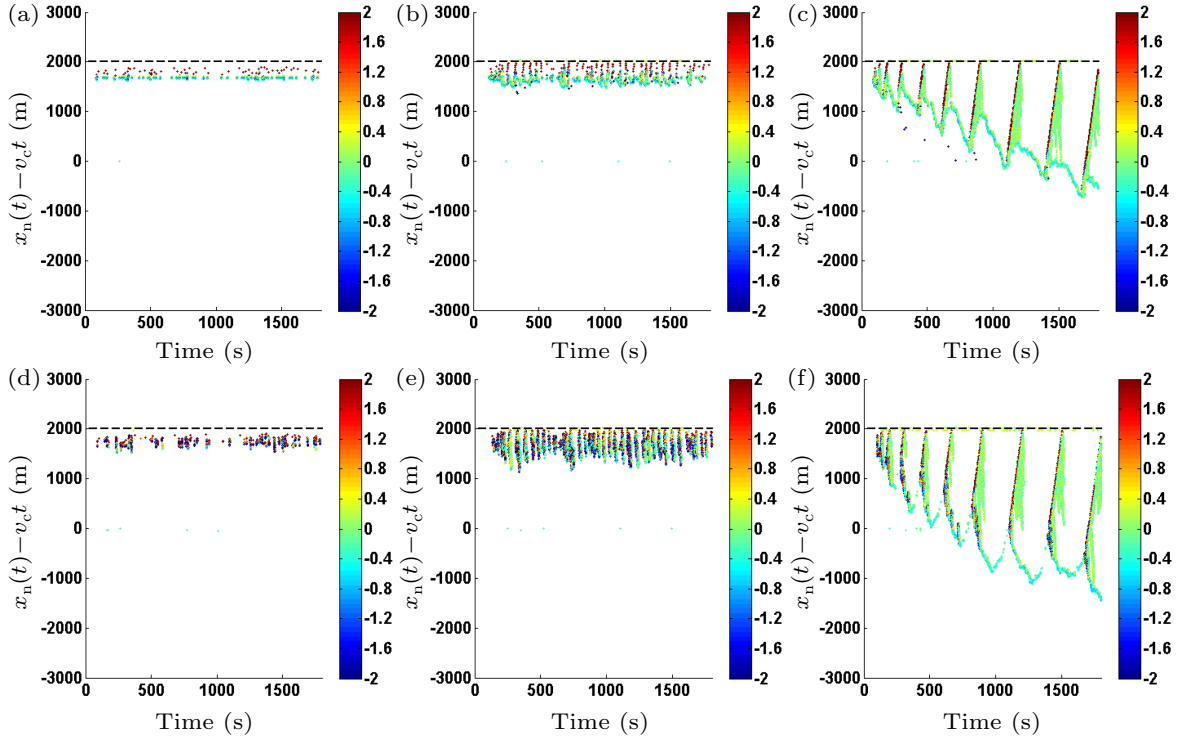


Fig. 14. The spatiotemporal pattern of notable jerks ($|J| > 0.1$ m/s^3) on panels (a)–(c) lane 1 and panels (d)–(f) lane 2 under the benchmark with $v_c = 10$ m/s at (a) and (d) $p_0 = 0.02$, (b) and (e) $p_0 = 0.04$, (c) and (f) $p_0 = 0.09$.

Figure 15 shows the notable jerks with $|J| > 0.1$ m/s^3 under the benchmark when $v_c = 20$ m/s. One can see that when $p_0 \approx 0.04$, due to a small speed difference between v_c and v_{max}, the 'acceleration- deceleration' process is weaken. Therefore, the comfort level index monotonically increases with the inflow.

Finally, figures 16 and 17 shows the notable jerks with $|J| > 0.1$ m/s^3 on lane 1 at $v_c = 10$ m/s and $v_c = 20$ m/s, respectively. Since traffic flow on the two lanes is similar, we show the results on one lane. One can see that with the increase of inflow, the jerks become more remarkable. Therefore, the comfort level index gradually increases.

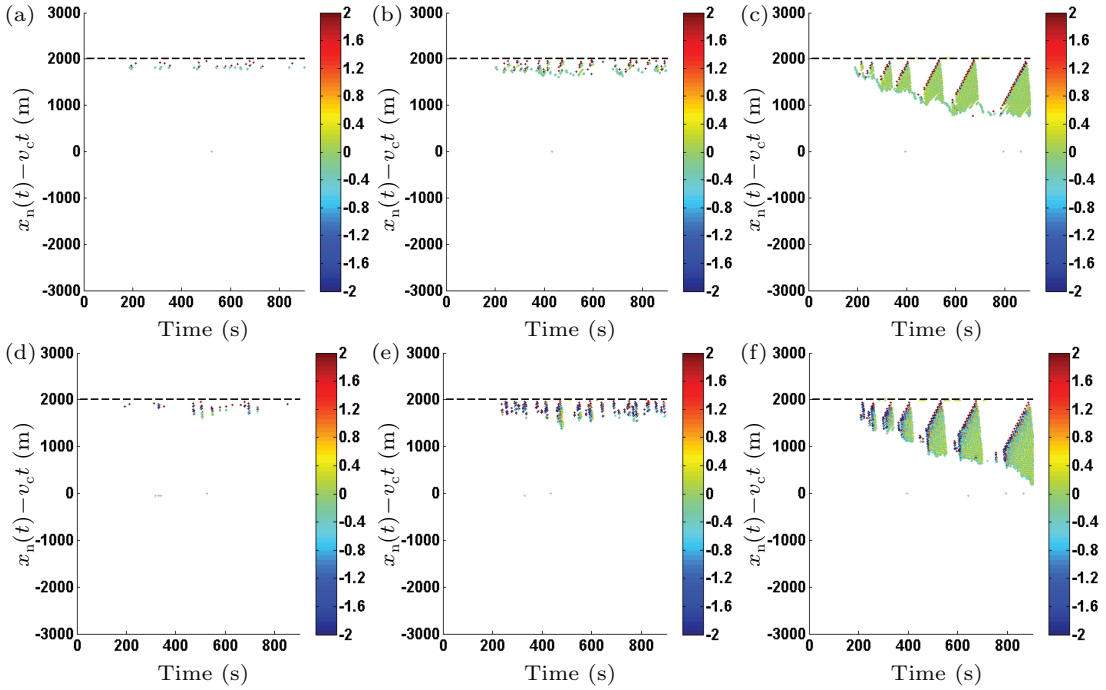


Fig. 15. The spatiotemporal pattern of notable jerks ($|J| > 0.1$ m/s^3) on panels (a)–(c) lane 1 and panels (d)–(f) lane 2 under the benchmark with $v_c = 20$ m/s at (a) and (d) $p_0 = 0.02$, (b) and (e) $p_0 = 0.04$, (c) and (f) $p_0 = 0.09$.

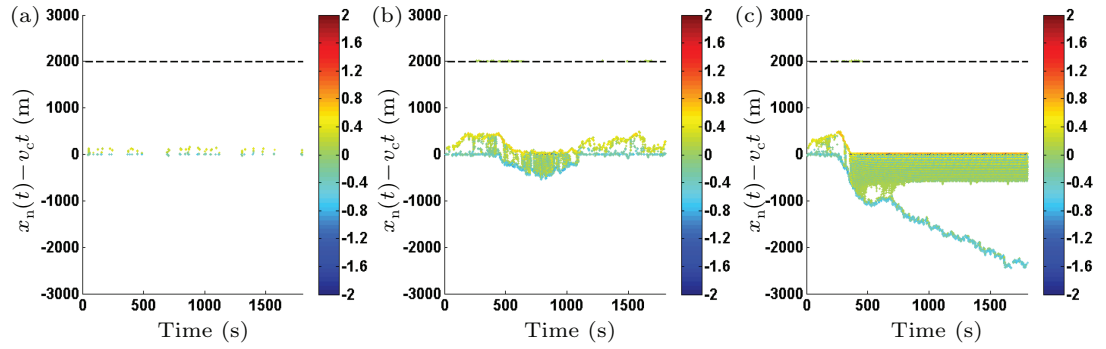


Fig. 16. The spatiotemporal pattern of notable jerks ($|J| > 0.1$ m/s^3) on lane 1 under the HRA with $v_c = 10$ m/s and $a_{cmd,lim} = -0.3$ m/s^2 at (a) $p_0 = 0.02$, (b) $p_0 = 0.07$, (c) $p_0 = 0.09$.

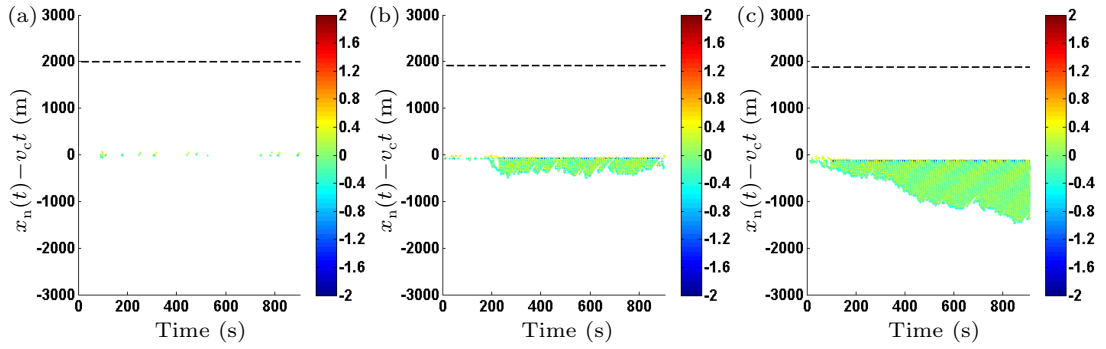


Fig. 17. The spatiotemporal pattern of notable jerks ($|J| > 0.1$ m/s^3) on lane 1 under HRA with $v_c = 20$ m/s and $a_{cmd,lim} = -0.3$ m/s^2 at (a) $p_0 = 0.02$, (b) $p_0 = 0.07$, (c) $p_0 = 0.09$.

4. Conclusion

This paper investigates the evolution of traffic flow of CAVs induced by a moving bottleneck on a two-lane highway. An HRA has been used to control the CAVs in the control zone. The overtaking throughput as well as the outflow rate, the travel delay, the fuel consumption, and the comfort level have been investigated to evaluate performance of the HRA. A comparison with the benchmark has been made, in which CAVs change lane in the control zone as long as lane changing condition is met.

Our study found that (i) The overtaking throughput and the outflow rate under the HRA are larger than that under the benchmark; (ii) The travel delay and fuel consumption under the HRA are always smaller; (iii) The comfort level under HRA could be always better than that under the benchmark.

In the future work, the study can be extended in several directions. (i) The optimization-based control algorithms need to be evaluated and compared with the HRA. (ii) The mixed traffic flow consisting of human-driven vehicles should be considered. (iii) The multilane highways should be investigated. (iv) The multi-moving bottlenecks should be studied. (v) The field test concerning CAV and moving bottleneck will be carried out.

Acknowledgment

Project supported by the National Natural Science Foundation of China (Grant Nos. 71931002 and 72288101).

References

[1] Shladover S E, Su D and Lu X Y 2012 *Transp. Res. Rec.* **2324** 63
[2] Milanes V, Shladover S E, Spring J, Nowakowski C, Kawazoe H and Nakamura M 2014 *IEEE Trans. Intel. Transp. Syst.* **15** 296
[3] Ding J S Y, Li L, Peng H and Zhang Y 2020 *IEEE Trans. Intel. Trans. Sys.* **21** 3436
[4] Zeng J W, Qian Y S, Wei X T and Feng X 2018 *Chin. Phys. B* **27** 124502
[5] Tang T Q, Huang H J and Shang H Y 2010 *Chin. Phys. B* **19** 050517
[6] Wan Q, Peng G Q, Li Z B and Inomata F H T 2020 *Transp. Res. Part C: Emer. Technol.* **117** 102682
[7] Liu H, Kan X, Shladover S E, Lu X Y and Ferlis R E 2018 *J. Intel. Transp. Sys.* **22** 263
[8] Hua X D, Wang W and Wang H 2016 *Acta Phys. Sin.* **65** 084503 (in Chinese)
[9] Marinescu D, Curn J, Bouroche M and Cahill V 2012 *Proceedings of 2012 15th International IEEE Conference on Intelligent Transportation Systems*, September 16–19, 2012, Anchorage, AK, USA, 13115311
[10] Xin Q, Fu R, Ukkusuri S V, Yu S W and Jiang R 2021 *Physica A* **563** 125452
[11] Xie D F, Gao Z Y and Zhao X M 2010 *Chin. Phys. B* **19** 080515
[12] Uno A, Sakaguchi T and Tsugawa S 1999 *Proceedings of 1999 IEEE/IEEJ/JSAI International Conference on Intelligent Transportation Systems*, October 5–8, 1999, Tokyo, Japan, pp. 783–787
[13] Lu X Y and Hedrick J K 2003 *Inter. J. Cont.* **76** 193
[14] Lu X Y, Tan H S, Shladover S E and Hedrick J K 2004 *Veh. Sys. Dyn.* **41** 85
[15] Xu H L, Zhang Y, Cassandras C G, Li L and Feng S 2020 *Trans. Res. Part C: Emer. Technol.* **120** 102773
[16] Rios-Torres J and Malikopoulos A A 2017 *IEEE Trans. Intel. Transp. Sys.* **18** 780
[17] Ntousakis I A, Nikolos I K and Papageorgiou M 2016 *Transp. Res. Part C: Emer. Technol.* **71** 464
[18] Letter C and Elefteriadou L 2017 *Transp. Res. Part C: Emer. Technol.* **80** 190
[19] Dong C Y, Chen Y J, Wang H, Ni D H, Shi X M and Lyu K Y 2022 *IEEE Trans. Veh. Tech.* 1–15
[20] Zhang T Y, Zhang J X, Lu M Y, Lin W H and Cong Z 2018 *Proceedings of* 2018 *3rd International Conference on Smart City and Systems Engineering,* December 29–30, 2018, Xiamen, China, 18638001
[21] Zheng Y and Hansen J H L 2017 *IEEE Trans. Intel. Vehicles* **2** 14
[22] You C X, Lu J B, Filev D and Tsiotras P 2019 *Robot. Auto. Sys.* **114** 1
[23] Guo J Q, Cheng S L and Liu Y Z X 2020 *IEEE Trans. Intel. Transp. Sys.* **22** 1639
[24] Dong C Y, Wang H, Li Y, Wang W and Zhang Z 2019 *IEEE Trans. Intel. Trans. Syst.* 1–13
[25] Wang B J, Li W, Wen H S and Hu X J 2021 *Physica A* **573** 125852
[26] Zheng Y, Ran B, Qu X and Zhang J 2019 *IEEE Trans. Intel. Trans. Syst.* 1–10
[27] Ehsan A, Aschkan O, Lily E 2021 *Transp. Res. Part C: Emer. Technol.* **126** 103072
[28] Nagalur Subraveti H H S, Srivastava A, Ahn S, Knoop V L and van Arem B 2021 *Transp. Res. Part C: Emer. Technol.* **127** 103126
[29] Yang C, Chen X D, L X and Li Meng 2022 *Transp. Res. Part C: Emer. Technol.* **144** 103864
[30] Zhu L, Lu L J, Wang X N, Jiang C M and Ye N F 2022 *IEEE Trans. Intel. Trans. Syst.* **23** 8
[31] Gazis D C and Herman R 1992 *Transp. Sci.* **26** 223
[32] Newell G F 1998 *Transp. Res. Part B: Method.* **32** 531
[33] Fang Y, Chen J Z and Peng Z Y 2013 *Chin. Phys. B* **22** 108902
[34] Hu X J, Lin C X, Hao X T, Lu R Y and Liu T H 2021 *Physica A* **584** 126335
[35] Simoni M D and Claudel C G 2017 *Transp. Res. Part B: Method.* **104** 238
[36] Piacentini G, Ferrara A, Papamichail I and Papageorgiou M 2019 *Proceedings of 2019 IEEE 58th Conference on Decision and Control,* December 11–13, 2019, Nice, France, 19450254
[37] Liu H Q and Jiang R 2021 *Physica A* **575** 126055
[38] Liu H Q, Jiang R, Tian J F and Zhu K X 2023 *Chin. Phys. B* **32** 014501
[39] Arem B V, Driel C J G V and Visser R 2006 *IEEE Trans. Intel. Transp. Syst.* **7** 4
[40] Omae M, Fukuda R, Ogitsu T and Chiang W P 2014 *Inter. J. Intel. Trans. Syst. Res.* **12** 3
[41] Tian B, Wang G Q, Xu Z G, Zhang Y Q and Zhao X M 2021 *Vehi. Commun.* **29** 100333
[42] Zhang Y Q, Tian B, Xu Z G, Gong S Y, Gao Y, Cui Z C and Chen X G 2022 *Trans. Res. Part C: Emer. Technol.* **142** 103766
[43] Wang Y P, Wei L and Chen P 2020 *Trans. Res. Part C: Emer. Technol.* **111** 135
[44] Jia D Y and D Ngoduy 2016 *Trans. Res. Part C: Emer. Technol.* **68** 245
[45] Wang M 2018 *Trans. Res. Part C: Emer. Technol.* **91** 276
[46] Hu X W and Sun J 2019 *Trans. Res. Part C: Emer. Technol.* **101** 111
[47] Luo Y G, Yong Y X, Cao K and Li K Q 2016 *Trans. Res. Part C: Emer. Technol.* **62** 87
[48] Li X P, Cui J X, An S and Parsafard M 2014 *Transp. Res. Part B: Method.* **70** 319
[49] Ma J Q, Li X P, Zhou F, Hu J and BB Park 2017 *Transp. Res. Part B: Method.* **95** 421
[50] Guo Y, Ma J Q, Xiong C F, Li X P, Zhou F and Hao W 2019 *Trans. Res. Part C: Emer. Technol.* **98** 54
[51] Ntousakis I A, Nikolos I K and Papageorgiou M 2016 *Transp. Res. Part C: Emer. Technol.* **71** 464